Multi-band & temporal analysis of lensed blazar PKS 1830-211

MIT Haystack Observatory REU 2023

MIT HAYSTACK OBSERVATORY

Sophia Rubens[1,2], Dongjin Kim[1], Kazunori Akiyama[1], Vincent Fish[1]

[1] MIT Haystack Observatory [2] Dartmouth College

1. Abstract

This project is aimed at understanding the relationship between the low-energy (radio) and high-energy (γ-ray) emissions from the blazar PKS 1830-211, leveraging its unique gravitational lensing effects. The lensed components, NE and SW, are distinguished by their notable time delay (~26 days) and magnification ratios, making them valuable tools to study the background blazar. Using time-monitoring light curve data and high–angular resolution VLBI radio data observed during an unprecedented γ-ray flaring event, we aim to characterize the physical mechanisms responsible for these phenomena. We have identified γ-ray flaring patterns, some linked to radio activities and others not. Non-associated flares likely result from microlensing, while related ones are due to inverse Compton scattering in the jet. Multi-frequency VLBI images show varying magnification of lensed radio components during these flares, suggesting a chromatic jet structure and evolving jet core emissions, possibly due to the jet core's opacity effect.

2. Background and methodology

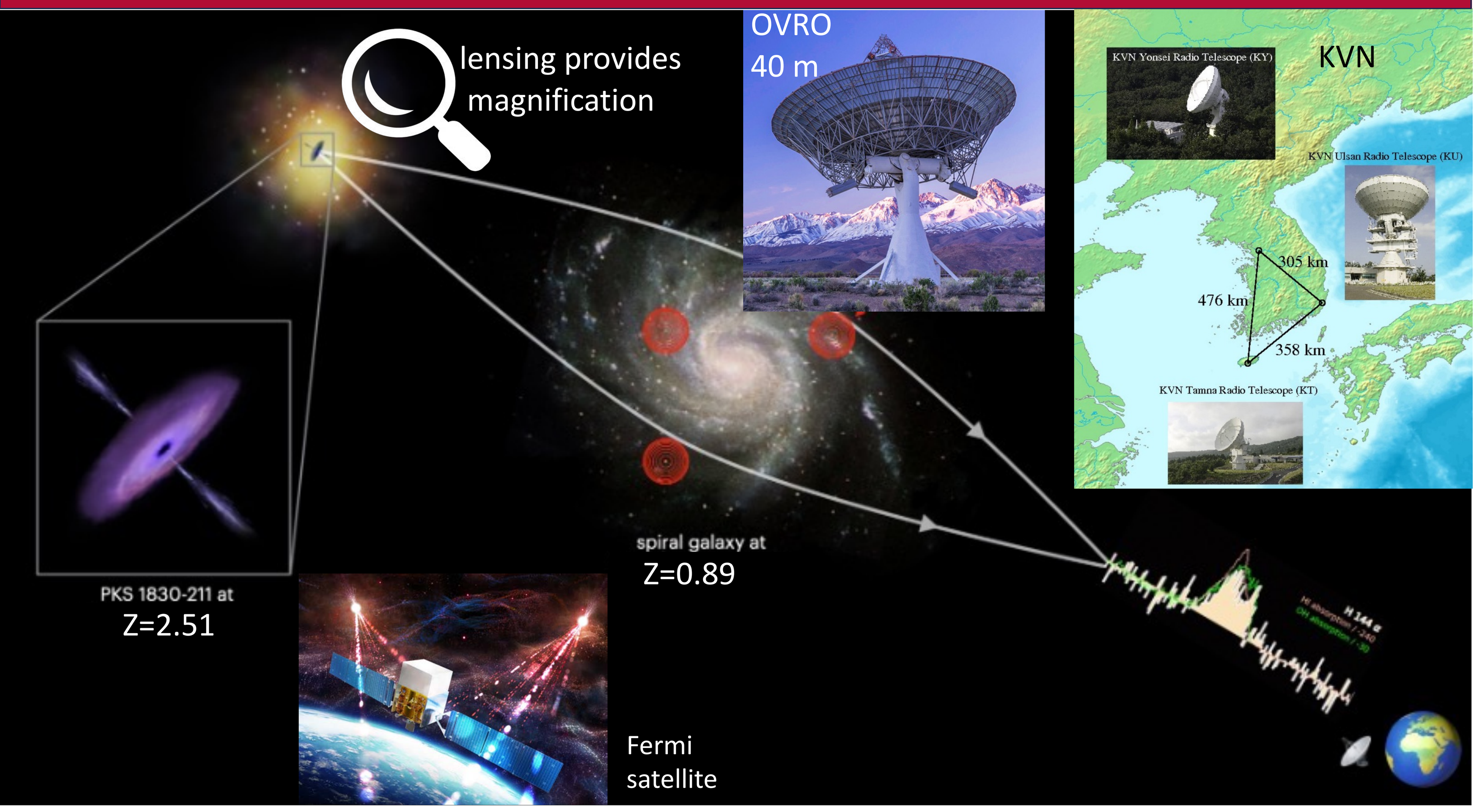

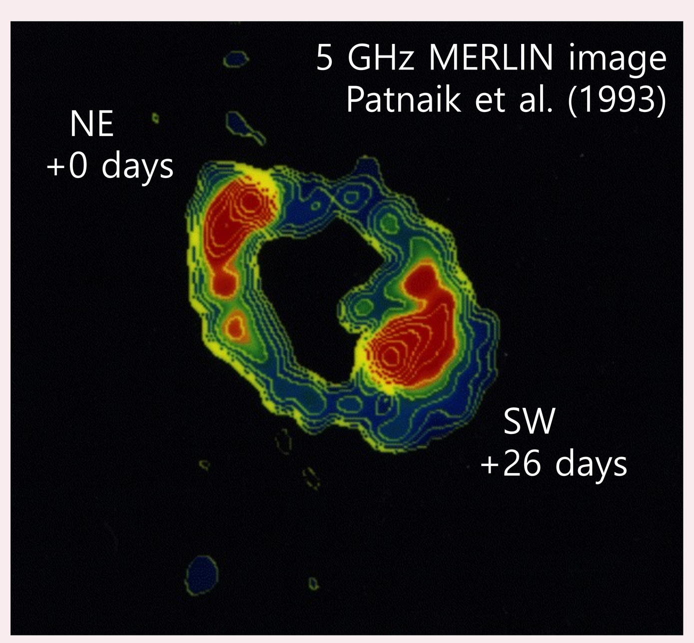

Very-long baseline interferometry (**VLBI**) aperture synthesis techniques to combine the signals from several antennas with large separations in order to achieve higher angular resolution at radio frequencies than would be possible with a single antenna. Here, the Astronomical image processing system (**AIPS**) is used for data reduction and the Caltech VLBI package implementation of the difference mapping technique (**difmap**) is used for imaging.

$$b(t) = \int_{-\infty}^{\infty} a(t-\tau)\Psi(\tau)d\tau$$

$$UDCF_{ij} = \frac{(a_i - \bar{a})(b_j - \bar{b})}{\sqrt{(\sigma_a^2 - e_a^2)(\sigma_b^2 - e_b^2)}}$$

$$DCF(\tau) = \frac{1}{M} UDCF_{ij}$$

The **discrete correlation function** permits the calculation of the correlation coefficients for a range of possible time delays for two time series. The **PyDCF** implementation is used here.

The **Lomb-Scargle periodogram** generalizes periodogram analysis to accommodate unevenly-sampled time series. The **scipy** implementation is used here.

$$P_{LS}(f) = \frac{1}{2}\{(\sum_n g_n \cos(2\pi f[t_n - \tau]))^2 / \sum_n \cos^2(2\pi f[t_n-\tau]) + (\sum_n g_n \sin(2\pi f[t_n - \tau]))^2 / \sum_n \sin^2(2\pi f[t_n-\tau])\}$$

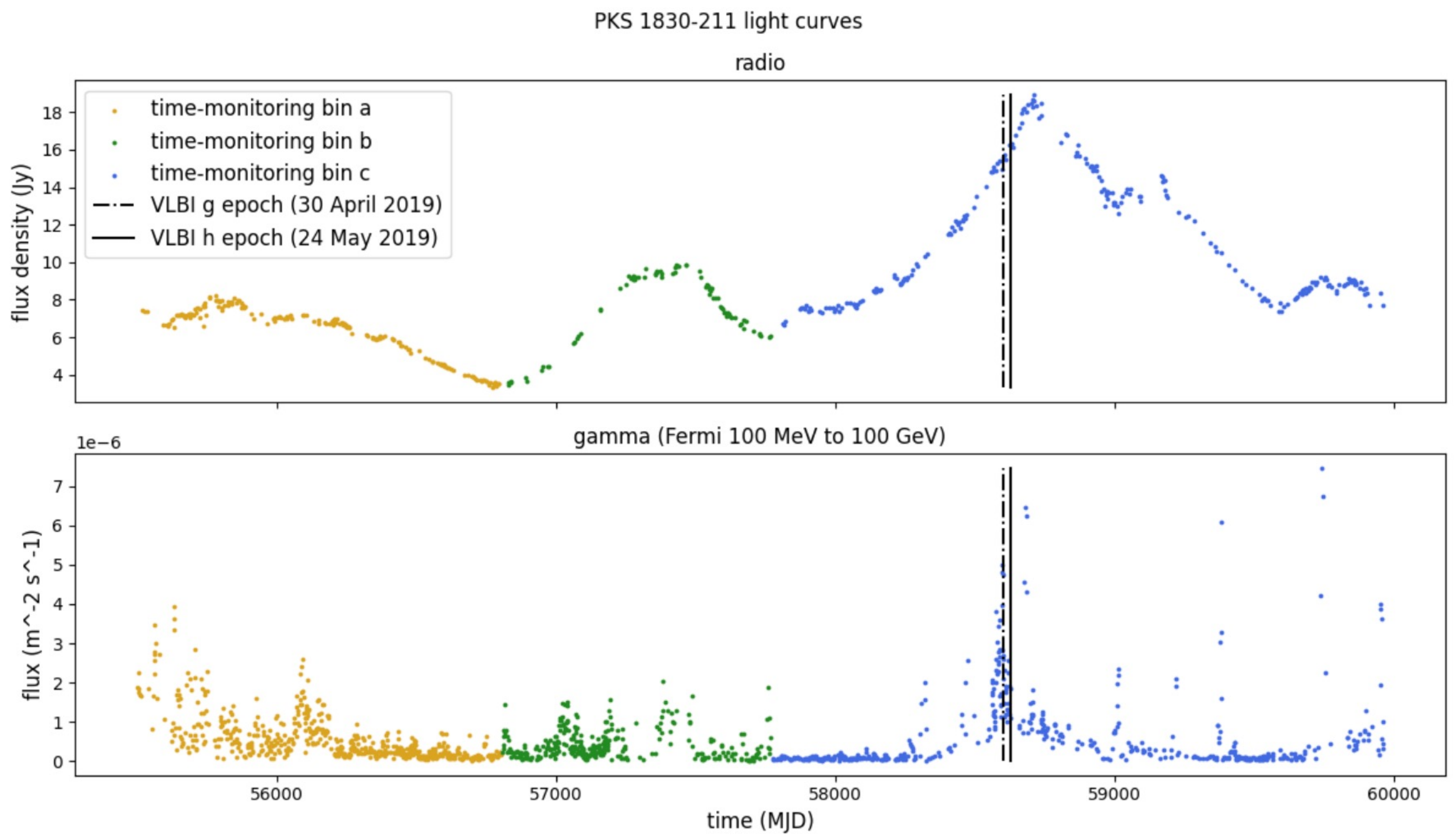

ABOVE: Side-by-side radio and γ-ray 14-year light curves. Colors indicate time bins corresponding to radio flares and vertical lines indicate VLBI observation epochs

RIGHT: inset of the Fermi light curve offering a closer look at the vicinity of the significant γ-ray–only significant flare.

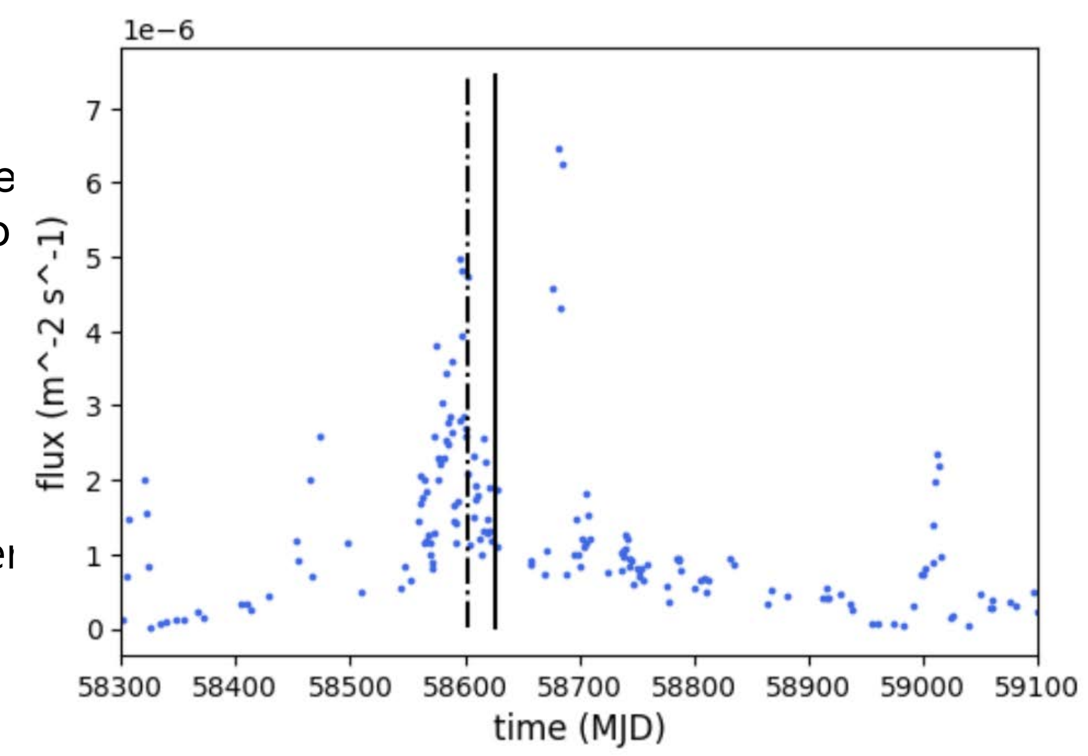

3. Results

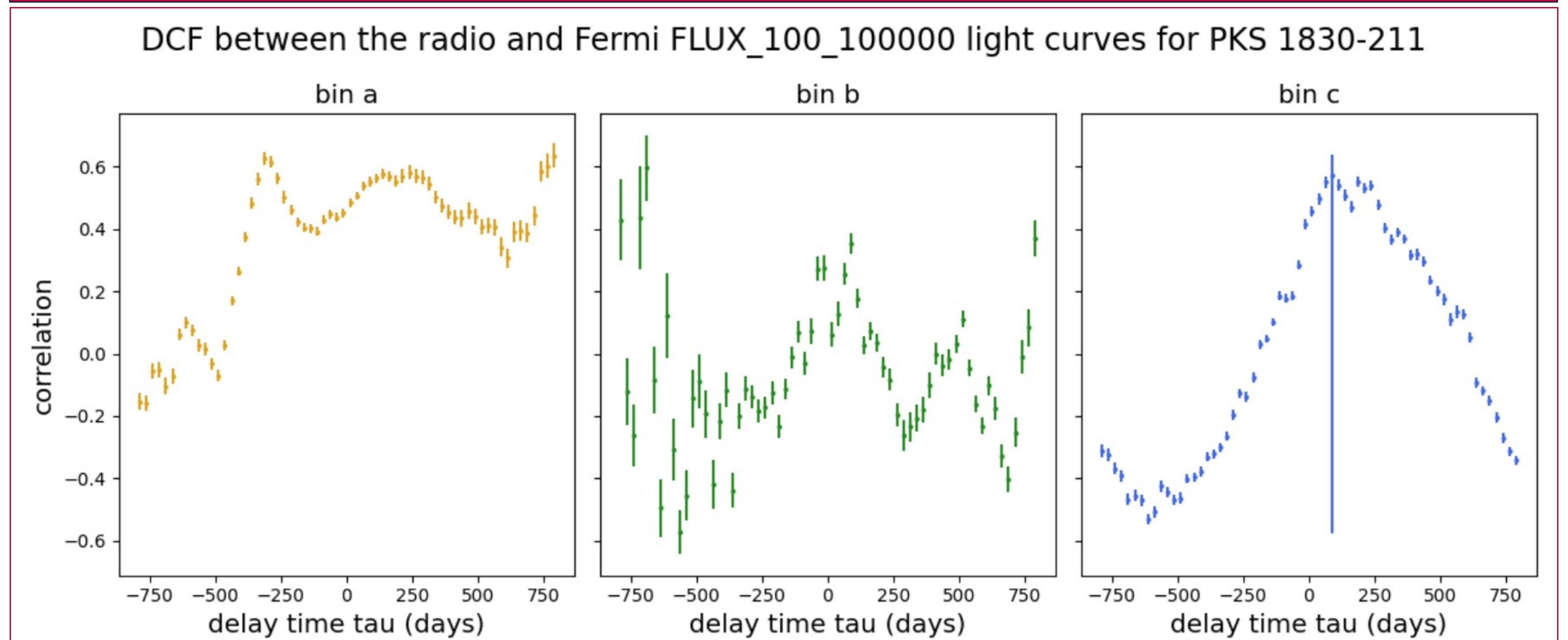

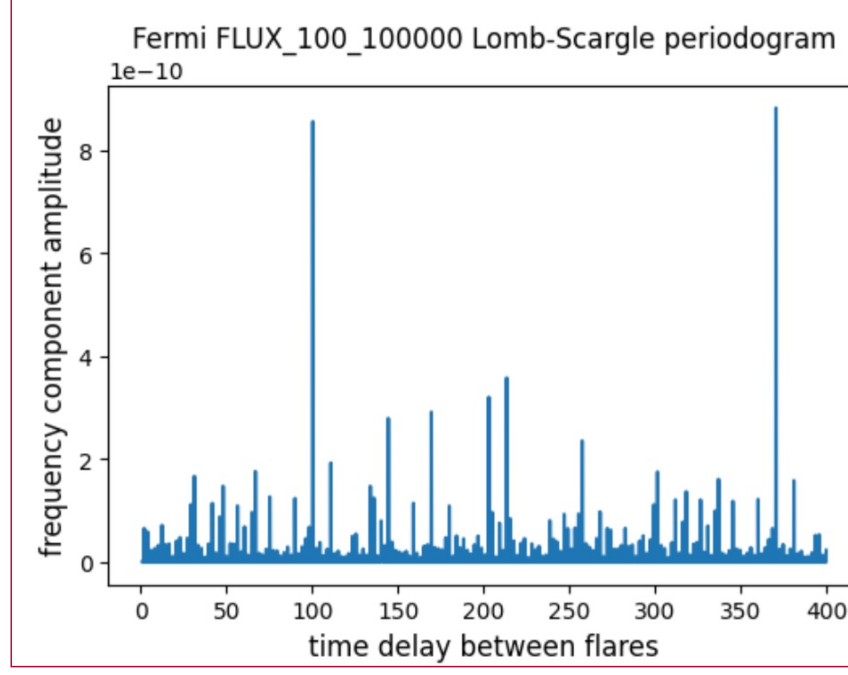

ABOVE: DCF analysis with a bin width of 25 days, delay values between -800 and 800 days, and LCs binned according to three radio flares. Noise in the power spectral density (PSD) limited the efficacy of initial attempts to determine the statistical significance of these results via Monte Carlo comparison with artificial LCs.

LEFT: The gamma LC exhibits a tentative periodicity of about 371 days, pending confidence interval determination.

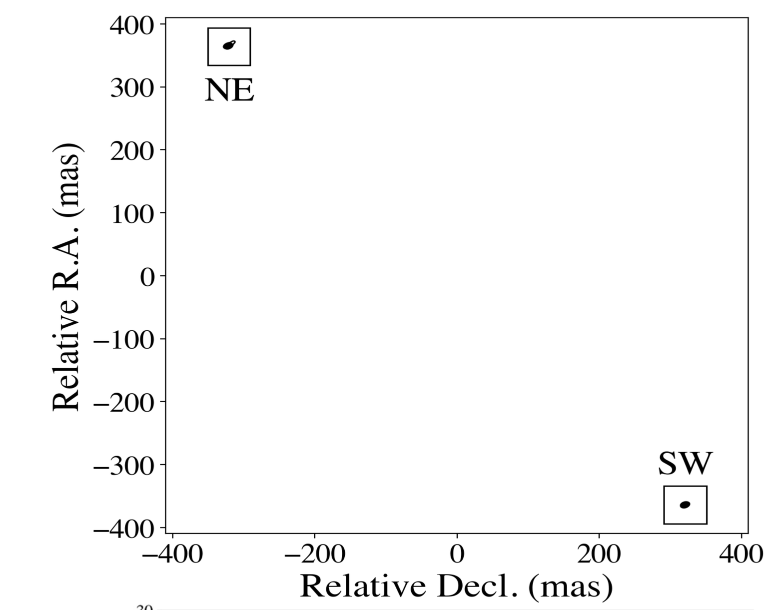

The northeastern (NE) and southwestern (SW) component of the lensed image of PKS 1830-211. The jet core is visible in both components, and an extended jet is visible in some images of the NE component.

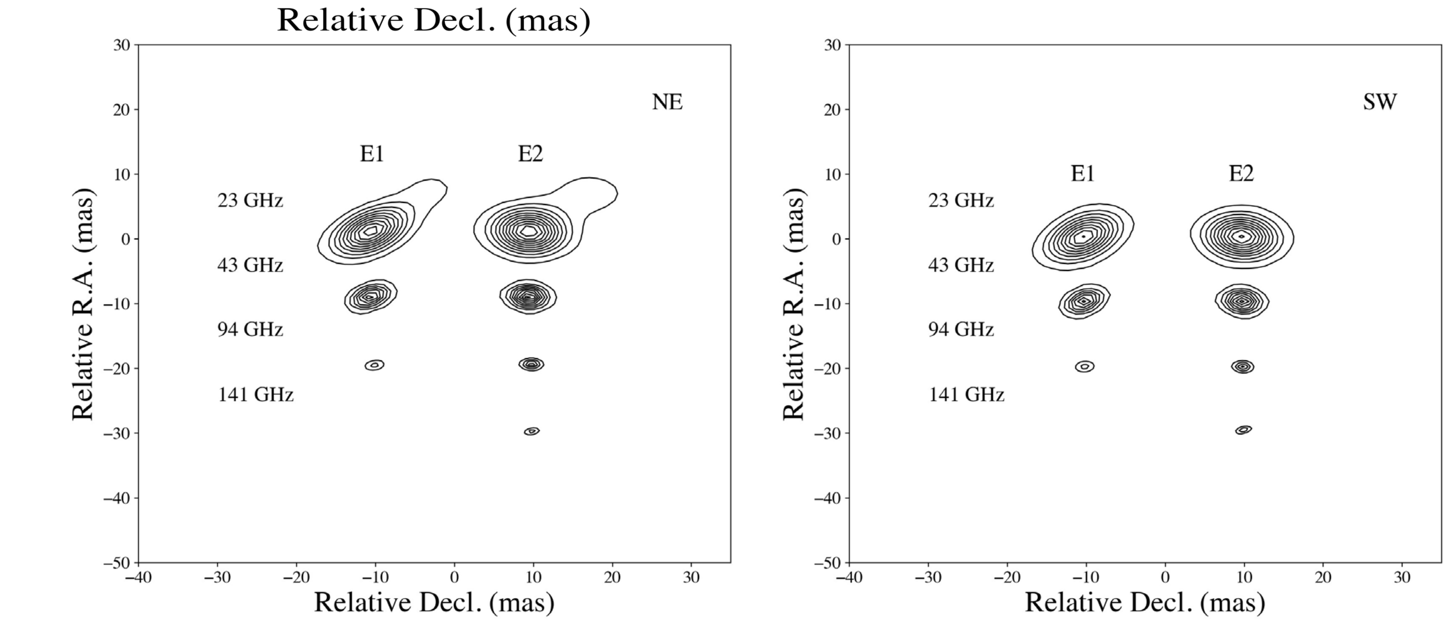

BELOW: Inclement weather during E1 curtailed data quality at higher frequencies, resulting in a non-detection at 141 GHz and significant sidelobes in the 94 GHz image. The gray region corresponds to the expectation set by Martí-Vidal et al. (ALMA 86 GHz monitoring)

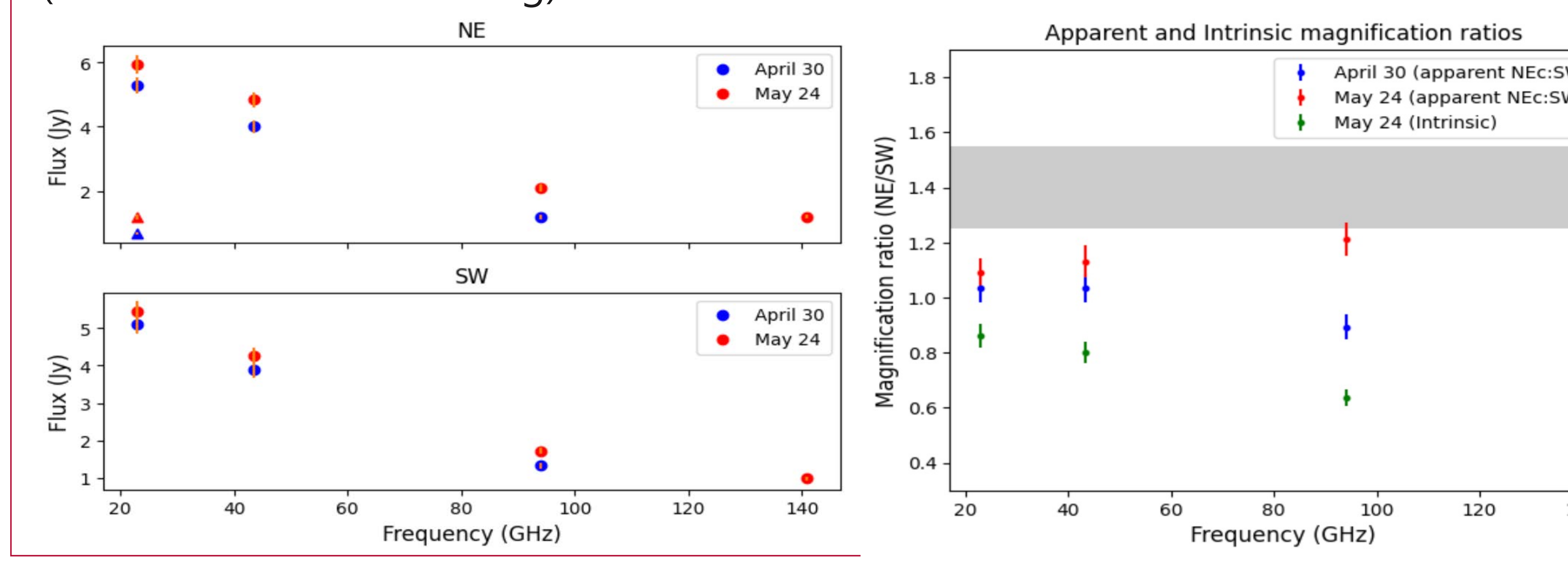

4. Conclusions

87-day delay between "bumps" in the radio and γ-ray light curves	→ inverse Compton scattering in the innermost region and moving shock waves in the radio jet
γ-ray burst with neither a delayed γ-ray nor radio counterpart	→ microlensing of γ-ray emission due to its small size in comparison to the radio region of the jet
frequency-dependent magnification ratio between lensed components	→ frequency-dependent opacity effect causes chromatic radio jet structure
smaller magnification ratios during the burst compared to previous studies	→ Intrinsic radio core variation during the flaring event

5. References

Joshi, M., Marscher, A. P., et al. 2014. The Astrophysical Journal, 785(2):132.
Emmanoulopolous, D., McHardy, I. M., & Papadakis, I. E., 2013. Monthly Notices of the Royal Astronomical Society. 433(2):907–927.
Martí-Vidal, I., Muller, S., et al. 2013. Astronomy & Astrophysics. 558:A123.
VanderPlas, J. T., 2018. The Astrophysical Journal Supplement Series. 236(1).
Schneider, P. 2015, Springer Berlin Heidelberg. Extragalactic Astronomy and Cosmology: an Introduction.
Edelson, R. A., & Krolik, J. H. 1988. The Astrophysical Journal. 333:646–659
Subramanyam, J. 2019. Chalmers University of Technology Masters thesis.
Böttcher et al., 2019. Galaxies. 7, 20.
Patnaik, A. R., Muxlow, T. W. B., & Jauncey, D. L., 1993. Liege International Astrophysical Colloquia. 31:363.